Dual-target inhibitors of the folate pathway inhibit intrinsically trimethoprim-resistant DfrB dihydrofolate reductases

Jacynthe L. Toulouse[1,2,3], Genbin Shi[4], Claudèle Lemay-St-Denis[1,2,3], Maximilian C. C. J. C. Ebert[5], Daniel Deon[6], Marc Gagnon[6], Edward Ruediger[6], Kévin Saint-Jacques[7], Delphine Forge[8], Jean Jacques Vanden Eynde[8], Anne Marinier[6], Xinhua Ji[4] and Joelle N. Pelletier[1,2,3,9*]

CONTENTS

Table S1. Protein sequence identity and query coverage (in brackets) of DfrBs with the expected value [a] (e-value, in bold).

	DfrB1	DfrB2	DfrB3	DfrB4	DfrB5	DfrB6	DfrB7	DfrB9
DfrB1	100%	98% (79%) **6e-49**	79% (98%) **9e-49**	78% (98%) **7e-48**	88% (100%) **7e-54**	87% (100%) **3e-52**	88% (100%) **2e-53**	78% (98%) **9e-48**
DfrB2		100%	86% (100%) **8e-50**	74% (100%) **6e-46**	81% (98%) **8e-49**	83% (98%) **1e-48**	79% (98%) **2e-48**	85% (100%) **2e-50**
DfrB3			100%	79% (100%) **2e-48**	83% (98%) **5e-50**	84% (98%) **3e-49**	81% (98%) **6e-49**	85% (100%) **1e-50**
DfrB4				100%	78% (98%) **4e-49**	78% (98%) **7e-47**	77% (98%) **1e-48**	74% (100%) **3e-46**
DfrB5					100%	91% (100%) **2e-54**	94% (100%) **2e-56**	78% (98%) **1e-47**
DfrB6						100%	91% (100%) **5e-54**	81% (98%) **8e-48**
DfrB7							100%	77% (93%) **3e-47**
DfrB9								100%

[a] The expected value (e-value) represents the probability of randomly matching two different sequences. The lower the e-value, the more significant the match.

Table S2. IC_{50} of His_6-DfrB1 and HPPK with inhibitors **1** to **5**.

	IC_{50} (μM) [a]				
Inhibitor	**1**	**2**	**3**	**4**	**5**
His_6-DfrB1	650 ± 87	580 ± 140	520 ± 62	330 ± 19	550 ± 120
HPPK [b]	3.2 ± 0.3	9.5 ± 1.0	11.0 ± 3.0	25.5 ± 7.5	18.5 ± 4.3

[a] Values are given as the average ± standard deviation from the mean of at least triplicates of two independent experiments.

[b] Values reported in reference (1).

Table S3. IC_{50} of DfrB1 (untagged) with TMP and inhibitors **1, 3**, **6** and **7**.

	IC_{50} (μM) [a]				
Inhibitor	TMP	**1**	**3**	**6**	**7**
DfrB1	$(12 \pm 3) \times 10^3$	1300 ± 940	440 ± 47	170 ± 55	590 ± 62

[a] Values are given as the average ± standard deviation from the mean of at least triplicates of two independent experiments.

Table S4. Total activity, yield and purity of DfrB purifications. [a]

	Total activity (U/200 mL) [b,c]	Yield (mg/200 mL) [c]	Purity (%)
DfrB1	3.7	9.0	**95**
DfrB2	8.5	11.0	**> 99**
DfrB3	4.4	7.8	**95**
DfrB4	1.9	6.2	**95**
DfrB5	8.2	12.4	**99**
DfrB7[c]	5.4	9.7	**96**

[a] DfrB1 and DfrB4 were purified by treatment at 75°C followed by a size-exclusion purification step whereas other DfrBs were purified by treatment at 65°C followed by a size-exclusion purification step, then by a second treatment at 75°C.

[b] 1 unit (U) is defined as the concentration of substrate converted to product per minute (μM/min).

[c] Per 200 mL of expression medium.

Table S5. Theoretical and measured masses of purified DfrBs.

DfrBs	Theoretical mass (Da) [a]	Measured mass (Da) [b]
DfrB1	8,446.4	8,446.4
DfrB2[c]	8,064.0	8,063.1
DfrB3	8,328.4	8,328.3
DfrB4	8,410.4	8,410.1
DfrB5	8,386.5	8,386.3
DfrB7	8,701.8	8,701.3

[a] Calculated from amino acid sequence with ExPASy Bioinformatics Resource Portal.

[b] Determined by mass spectroscopy.

[c] Missing the initiator methionine.

Table S6. k_{cat}^{NADPH} for the dihydrofolate reductase activity of DfrBs.

DfrB homolog	k_{cat}^{NADPH} (s^{-1}) [a]
DfrB1	0.32 ± 0.01
DfrB2	0.35 ± 0.01
DfrB3	0.18 ± 0.01
DfrB4	0.22 ± 0.01
DfrB5	0.28 ± 0.01
DfrB7	0.26 ± 0.01

[a] k_{cat} value calculated for the global reaction. Values are given as the average ± standard deviation from the mean of at least triplicates of two independent experiments.

Table S7. IC_{50} of DfrBs with TMP and inhibitors **1**, **3, 6** and **7**.

	IC_{50} (μM) [a]				
Inhibitor	TMP	**1**	**3**	**6**	**7**
DfrB2	$(13 \pm 1) \times 10^3$	790 ± 45	840 ± 230	170 ± 33	460 ± 14
DfrB3	$(18 \pm 4) \times 10^3$	480 ± 63	660 ± 68	93 ± 14	250 ± 81
DfrB4	$(16 \pm 2) \times 10^3$	540 ± 57	780 ± 15	190 ± 20	310 ± 35
DfrB5	$(22 \pm 5) \times 10^3$	850 ± 39	730 ± 12	130 ± 2	500 ± 54
DfrB7	$(12 \pm 2) \times 10^3$	980 ± 610	710 ± 190	130 ± 41	360 ± 130

[a] Values are given as the average ± standard deviation from the mean of at least triplicates of two independent experiments.

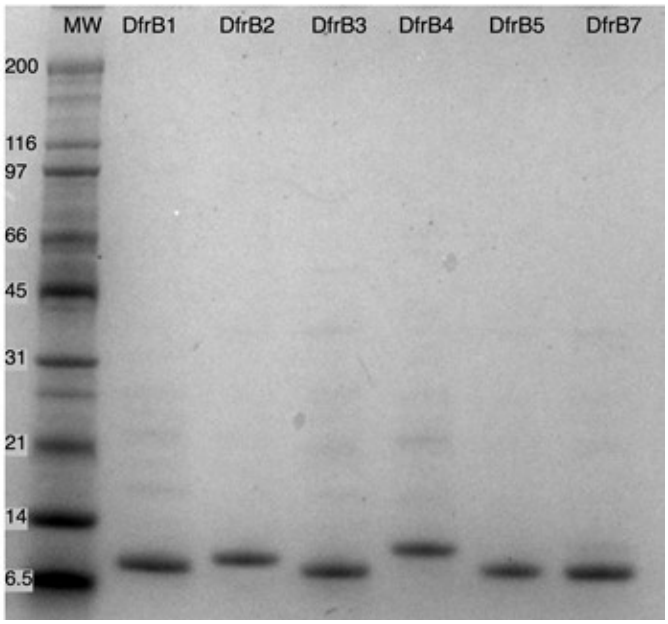

Figure S1. 12% SDS-PAGE gel of purified DfrBs. DfrB1 and DfrB4 were purified by treatment at 75°C followed by a size-exclusion purification step whereas other DfrBs were purified by treatment at 65°C followed by a size-exclusion purification step, then by a second treatment at 75°C. Purity was ≥ 95% (Table S4). MW: molecular weight markers.

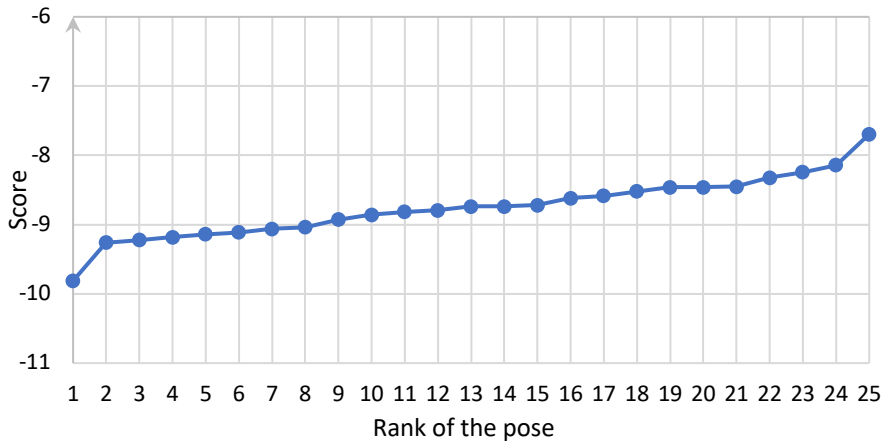

Figure S2. Scoring of the 25 top-ranked poses following docking of inhibitor 1 + NADPH onto DfrB1 (PDB:2RK1). The GBVI/WSA ΔG scoring function was applied. Pose 7 is illustrated in Figure 2 and discussed in the main text.

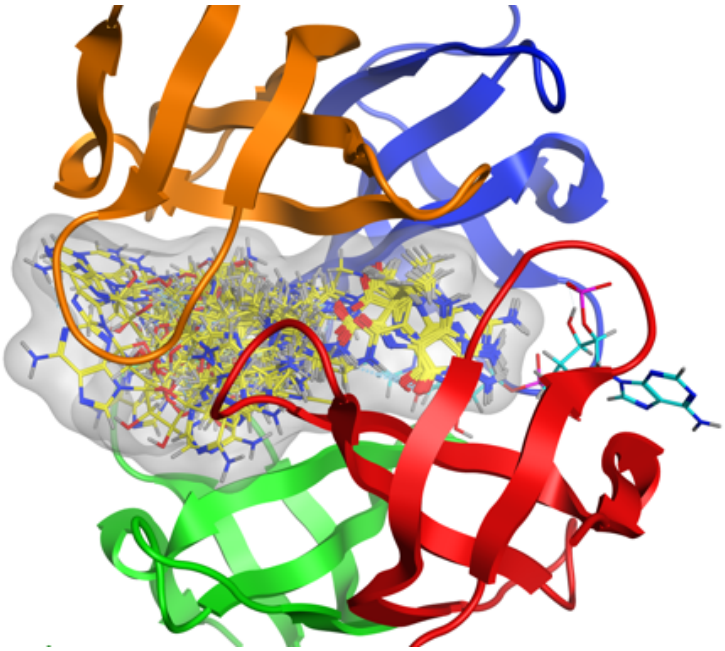

Figure S3. Docking of inhibitor 1 + NADPH onto DfrB1 (PDB:2RK1). Superposition of the 25 top-ranked poses of inhibitor **1** (yellow sticks) and NADPH (cyan sticks). The docking protocol allowed broad conformational sampling of the linker and adenosine moiety of **1**.

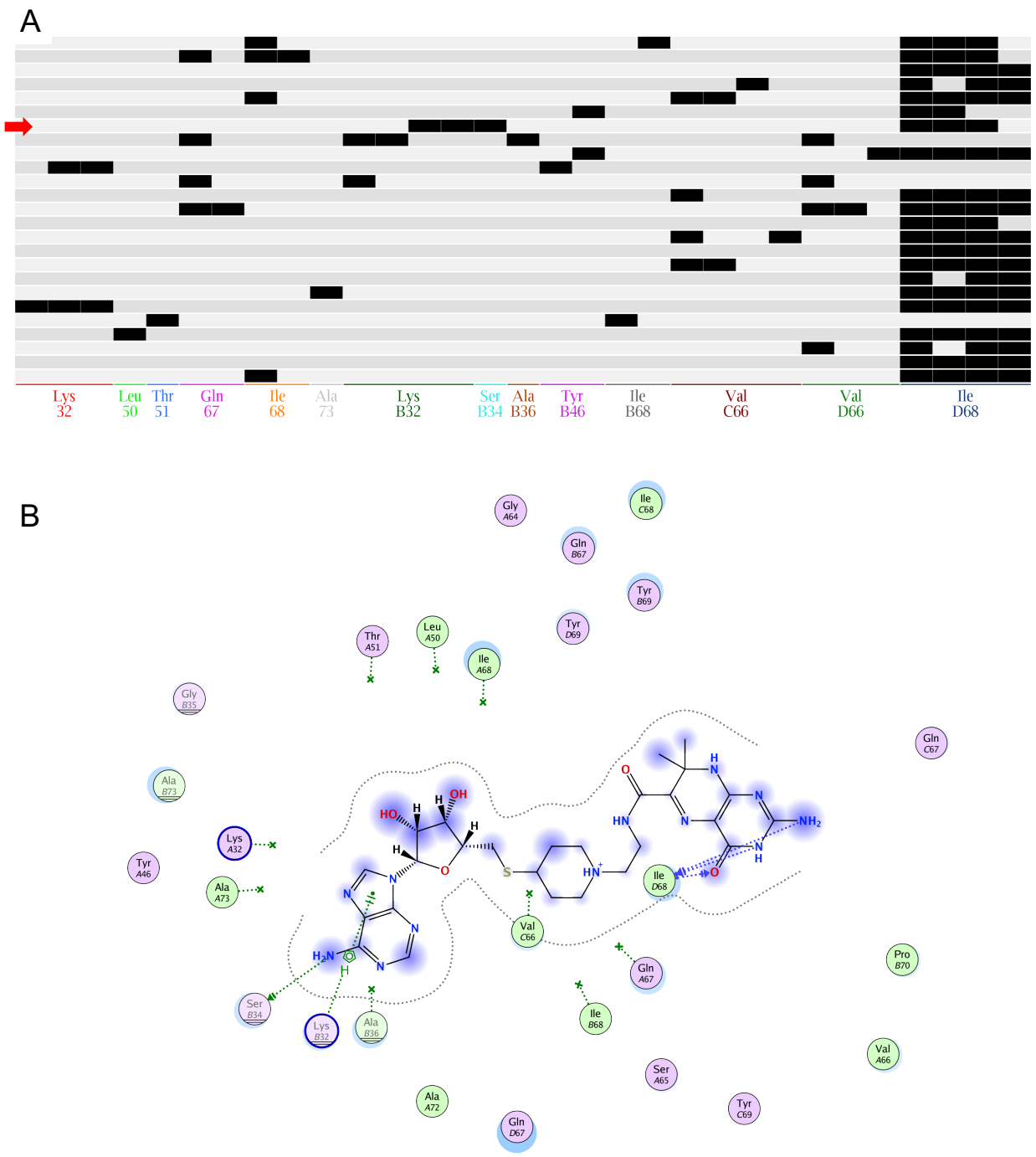

Figure S4. Protein Ligand Interaction Fingerprint (PLIF) for docking of inhibitor 1 + NADPH onto DfrB1 (PDB:2RK1). A) The interactions established between inhibitor **1** and DfrB1 for the top 25 poses of docked inhibitor 1 (Figure S3). Each pose is a horizontal line (alternating light/medium gray) and each interaction with inhibitor **1** is marked as a black rectangle above the corresponding amino acid. The width of the rectangle indicates the number of interactions established between the inhibitor and that residue. The 2nd to 4th protomers of DfrB1 are labelled B-D. **B)** PLIF for the representative pose of docked inhibitor 1, shown in Figure 2 and marked by a red arrow in Panel A. Residues with green dotted lines extending to inhibitor **1** establish contacts in this pose; short, green dotted lines terminated with an X indicate residues that establish contacts with inhibitor **1** in at least one other pose. The PLIF application in MOE2019 was used to generate the data and images.

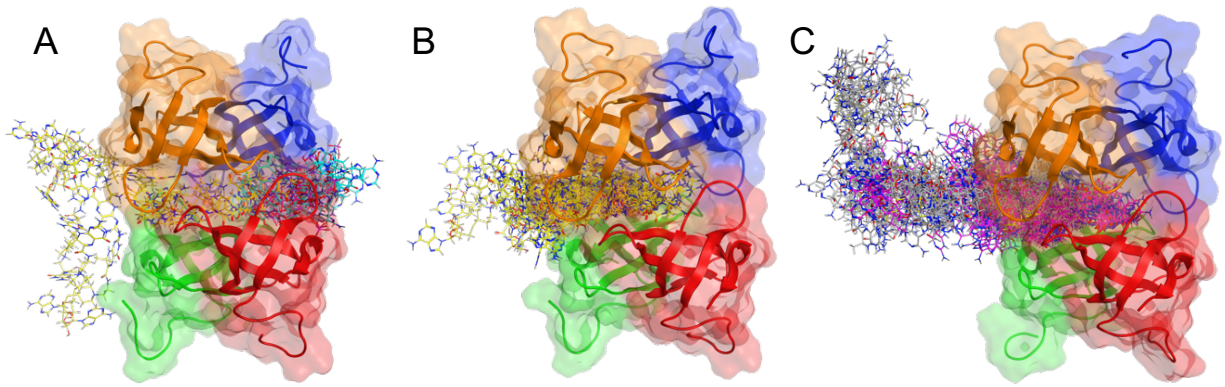

Figure S5. Exit of inhibitor 1 from the DfrB1 active-site tunnel (PDB: 2RK1). A) In the presence of NADPH, **1** (yellow sticks) exited from the tunnel whereas NADPH (cyan) remained at its binding site. **B)** The single molecule of **1** (yellow sticks) exited from the tunnel. **C)** Both molecules of **1** (grey and magenta sticks) exited from the same tunnel mouth.

Inhibitor Synthesis Schemes:

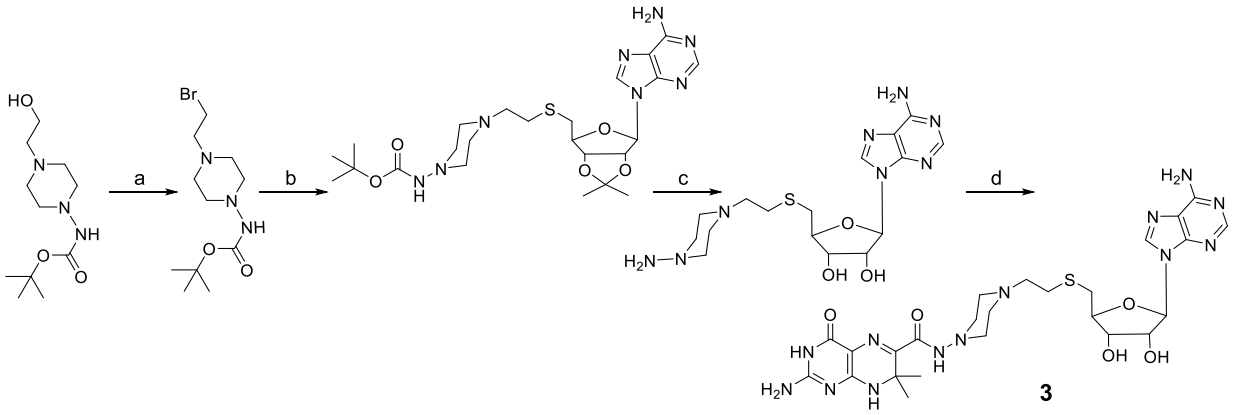

Scheme S1. Synthesis of bisubstrate inhibitor 3. Reagents and conditions: a) PPh_3, CBr_4, CH_2Cl. b) $NaOCH_3$, 2',3'-O-isopropylideneadenosine-5'-thioacetate. c) CF_3COOH, CH_2Cl_2, d) HATU base, 6-carboxy-7,7-dimethyl-7,8-dihydropterin, DIPEA, DMF. Yield: 22%. Purity: 95%.

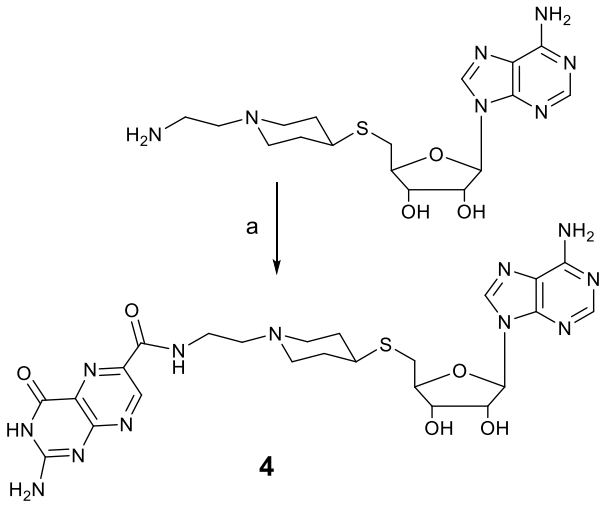

Scheme S2. Synthesis of bisubstrate inhibitor 4. Reagents and conditions: a) HATU base, 2-amino-4-oxo-3,4-dihydropteridine-6-carboxylic acid, DIPEA, DMF. Yield: 20%. Purity: 95%.

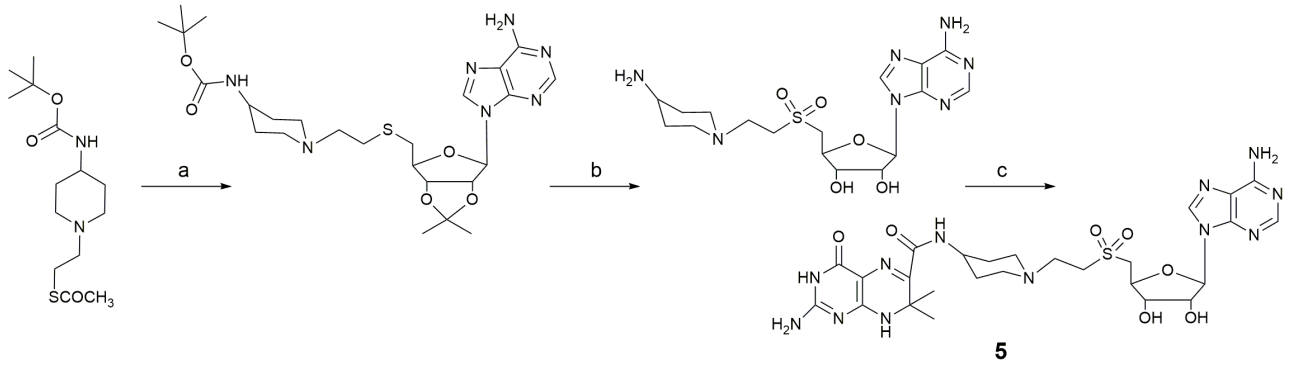

Scheme S3. Synthesis of bisubstrate inhibitor 5. Reagents and conditions: a) $NaOCH_3$, MeOH, 2',3'-O-isopropylideneadenosine-5'-thioacetate. b) Oxone, TFA, CH_2Cl_2 c) HATU base, 6-carboxy-7,7-dimethyl-7,8-dihydropterin, DIPEA, DMF. Yield: 18%. Purity: 95%.

Materials and methods

Materials.

Phusion Green High-Fidelity DNA Polymerase was purchased from Thermo Scientific (Waltham, MA, USA). Unless otherwise mentioned, restriction enzymes were purchased from New England Biolabs Canada (NEB) and oligonucleotide primers were synthesized by Alpha DNA, S.E.N.C. (Montreal, QC). Ligations were performed with the Takara DNA Ligation Kit Ver.2.1. Kanamycin was purchased from Teknova (Ontario, Canada) and TMP from Sigma Aldrich (Ontario, Canada). DNA sequencing was performed at the IRIC Genomic Platform at Université de Montréal. All

chemicals for the synthesis of **3**, **4** and **5** were purchased from MillporeSigma and TCI America. Dihydrofolate (DHF) was synthesized from folic acid as described(2) and stored as lyophilized aliquots at -80°C. β-NADPH was purchased from Chem-Impex (IL). All solvents were purchased from Fisher Chemicals.

Subcloning DfrBs for expression and purification.

His_6-DfrB1 and His_6-DfrB4 were obtained as previously reported(3). The genetic sequences encoding *dfrB2, dfrB3, dfrB5* and *dfrB7* were purchased from Bio Basic (Ontario, Canada) according to their respective GenBank accession numbers.(4) *DfrB* genes were obtained in pUC57 and subcloned into pET24 (Qiagen) for expression, as follows. A *dfrB* forward oligonucleotide primer (5'- AAAAACCGCGGCTAGCAAAGAGGAGAAATA-3') and two reverse oligonucleotide primers (DfrB2, DfrB5 and DfrB7: 5'- ATCGGATCCCGTCAGCTAATTAAGCTTTTA-3'; DfrB3: 5'- GACGGGCCCGTCAGCTAATTAAGCTTTTA-3') including the *HindIII* restriction site (underlined) served to PCR amplify each gene with Phusion Green High-Fidelity DNA Polymerase. The PCR products were digested with *NdeI* and *HindIII* and gel-extracted using the Monarch DNA gel extraction kit from NEB. The inserts were ligated into *NdeI*- and *HindIII*-digested pET24 for 30 minutes at 16°C. The DNA ligation products were transformed into competent *E. coli* DH5α by heat shock. The expected sequences of the final constructs were confirmed by DNA sequencing and transformed into *E. coli* BL21(DE3) (Qiagen) for expression.

To create the *dfrB4-pET24* construct (untagged), *His_6-DfrB4-pET24*(4) was used as a template for PCR amplification with a forward oligonucleotide primer (5'- AAAAAAAACATATGAATGAAGGAAAAAATGAGGTCAG-3') including a *NdeI* restriction site (underlined) and a reverse oligonucleotide primer (5'- AGCTAATTAAGCTTTTATCAGGCCACCC-3'; Sigma-Aldrich (Oakville, ON)) with a *HindIII* restriction site (underlined). The PCR product was purified and subcloned into pET24 and transformed as described above. The DNA sequence of the *dfrB4-pET24* construct was confirmed by sequencing.

To generate the *dfrB1-pET24* construct, a PCR method was used to remove the hexahistidine tag and the non-native13-residue *C*-terminal tail (ELGTPGRPAAKLN) from the WT R67 DHFR pQE32 construct.(5) A *NdeI* restriction site (underlined) was added using a forward oligonucleotide primer (5'- AAAAACCGCGGCTAGCAAAGAGGAGAAATAGCATATGAGAGGATCTCACCATCACC ATC-3'; Sigma-Aldrich (Oakville, ON)) and a *HindIII* restriction site (underlined) with a reverse oligonucleotide primer (5'- GGGAAGCTTTTAGTTGATGCGTTCAAGCGCC-3'; Sigma-Aldrich (Oakville, ON)). The PCR product was digested with *NdeI* and *HindIII* (Thermo Scientific, Waltham, MA) and purified using the PureLink Quick Gel Extraction and PCR Purification Combo Kit (Invitrogen, Carlsbad, CA). The digested fragment was subcloned into the *NdeI*- and *HindIII*-digested pET24 and transformed as described above. The sequence of the final construct was confirmed by DNA sequencing.

DfrB purification.

Recombinant DfrBs were overexpressed in *E. coli* BL21 (DE3) using ZYP-5052 autoinduction medium.(6) Bacteria were propagated in 200 mL for 2 h at 37°C then at 22°C for 16 h to allow overexpression (DfrB1: 3 × 200 mL; DfrB2, DfrB3, DfrB4 and DfrB5: 2 × 200 mL; DfrB7: 1 × 200 mL). The cells were harvested and lysed by sonication as previously described.(5) Lysates

were incubated at 65°C for 10 minutes (or at 75°C for DfrB1 and DfrB4) then chilled on ice for 10 minutes and centrifuged (10 minutes at 16,000 × *g*). The temperature was selected to maximize the ratio between the folded, soluble DfrB (in solution) and the unfolded, aggregated proteins in the lysate. The supernatants were concentrated to 1 mL using an Amicon concentrator (MWCO 3,000, Millipore) and injected on a Superose 12 size exclusion chromatography column (1.6 cm × 55 cm) pre-equilibrated with 0.05 mM potassium phosphate buffer, pH 7.0. DfrB-containing fractions were identified according to their activity using the standard spectrophotometric Dfr activity assay. Purity was determined by resolution on 12% SDS-PAGE. To improve purity, DfrB2, DfrB3, DfrB5 and DfrB7 were heated a second time at 75°C for 10 min and then chilled on ice for 10 min, followed by a centrifugation as above. Protein concentration was determined using the Bio-Rad protein assay (Bio-Rad, Hercules, CA). Purity was determined by resolution on 12% SDS-PAGE. The migration of the DfrBs upon SDS-PAGE does not directly reflect their molecular masses, which were confirmed by mass spectrometry (Regional Mass Spectrometry Centre at Université de Montréal) (Figure S1, Table S5).

DfrB kinetics.
The productive affinity (K_M), turnover number (k_{cat}) and the half maximal inhibitory concentration (IC_{50}) were determined as previously described.(7) The inhibition constant (K_i) was calculated by applying the Cheng-Prusoff equation(8) which relates IC_{50} to K_i. Values are the average ± standard deviation from the mean of at least triplicates of two independent experiments.

Determination of the binding stoichiometry of **1** was attempted as previously described,(9) with the following modifications. The concentration of **1** ranged from 200 µM to 1300 µM. Reactions were initiated with 7 mU of DfrB1. The change in absorbance at 340 nm resulting from the conversion of DHF and NADPH to tetrahydrofolate and $NADP^+$ was determined in 5 mm (instead of 10 mm) path-length cuvettes to compensate for the absorbance of **1**.

IC_{50} determination for HPPK.
The reaction mixture (50 µL final volume) contained 1 nM *E. coli* HPPK, 2 µM ATP, 1 µM HP, 5 mM $MgCl_2$, 25 mM DTT and a trace amount of [α-^{32}P]-ATP (~1 µCi) in 100 mM Tris, pH 8.3. The experiments were conducted at 30 °C. The reaction was initiated by addition of the enzyme and stopped after 30 min by the addition of 6 µL of 0.5 M EDTA. The radioactive reactant and product were separated by thin-layer chromatography, using a PEI-cellulose plastic plate (EMD) with 0.3 M KH_2PO_4 as the mobile phase, and quantified by a Phosphor-Imager system (Amersham Typhoon TRIO). Values are the average ± standard deviation from the mean of triplicates. The IC_{50} values were obtained by fitting the data to a logistic equation by nonlinear least-squares regression. K_i values were calculated according to the experimentally determined IC_{50} values, as described above.

Docking simulations of bisubstrate inhibitor **1** *into DfrB1*:

Building small-molecule input and DfrB1 structure preparation.
All molecules were sketched in ChemDraw Professional 16. All atomistic 3D coordinates at pH7 were generated using the Database Wash application in MOE2019 (Chemical Computing Group, Montreal). DfrB1 structure PDB:2RK1 was prepared using the QuickPrep application with default parameters. The so-generated protein complex was used as input structure to dock inhibitor **1**.

Building models of DfrB1-ligand complexes and molecular docking.
Docking was performed using the Dock application in MOE2019. Bisubstrate inhibitor **1** was docked using Template Forced docking of the pterin moiety onto the pterin moiety of DHF in the 2RK1 crystal structure. This methodology was used to build the DfrB1 complex with either one or two molecules of **1**, and the complex with **1** + NADPH, where NADPH was templated onto the co-crystallized $NADP^+$ and remained fixed. Refinement was done in Rigid Receptor mode and the top 25 poses from the GBVI/WSA ΔG scoring function were written to the output database.

Conformational exploration of ligands in the active-site tunnel.
Conformational exploration of each DfrB1-ligand complex was performed using the LowModeMD method(10) in MOE2019. For simulation of **1** + NADPH, the docking pose having the adenosine moiety of **1** overlaying best with that of NADPH served as the starting conformation (Figure 2); for inhibitor **1** alone or in two copies, the pose having **1** docked in a conformation most similar to the pterin of DHF in PDB:2RK1 was used (Figure S3). All ligand atoms were kept free whereas receptor atoms in the binding pocket (all residues of DfrB1 within 4.5 Å of ligand molecules) were tethered with 10 kcal/mol, starting from 0.25 Å deviation around the original coordinates. All DfrB1 residues within 4.5 Å of those tethered atoms were fixed and the remainder of the system was set to inert. The forcefield was AMBER10:EHT with R-Field solvation. All conformations with ΔE of 1000 kcal/mol compared to the lowest energy conformation were retained. The exploration was stopped after attaining 1000 conformations, after 100 consecutive conformations were generated that were already present in the dataset or when a ligand escaped from the binding pocket. The Protein Ligand Interaction Fingerprint (PLIF) application in MOE2019 was used to determine the average binding mode of **1** in DfrB1. The calculation was performed using the default parameters.

Inhibitor synthesis.
General procedure A. The selected adenosine or piperidine thioacetate derivative (0.10 mmol) in methanol (10 mL) was treated with a solution of $NaOCH_3$/MeOH (0.12 mmol) added dropwise under nitrogen and stirred at room temperature for 10 min. The solution was transferred to the previously synthetized *t*-butyl (4-(2-bromoethyl)piperazin-1-yl)carbamate (0.10 mmol) and heated at 60°C overnight. The reaction mixture was concentrated by rotary evaporation and extracted by CH_2Cl_2. The concentrated solution was purified by silica gel flash chromatography with CH_2Cl_2-methanol (0-20%).

General procedure B. The selected adenosine derivative (0.10 mmol) was added to a mixture of pterin derivative (0.10 mmol), *O*-(7-azabenzotriazol-1-yl)-1,1,3,3-tetramethyluronium hexafluorophosphate (HATU) (0.11 mmol) and *N*,*N*-diisopropylethylamine (DIPEA) (0.33 mmol) in anhydrous dimethylformamide (DMF) (10 mL). After 2 h at room temperature, the solvent was evaporated under high vacuum and the reaction residue was purified by Waters Prep 150 HPLC System, Phenomenex C18 columns (catalogue no. 00G-4436-P0-AX, 250 mm × 21.2 mm 10 μm particle size, 110 Å pore) at a flow rate of 20 mL/min. A binary solvent system consisting of A = 0.1% aqueous TFA and B = 0.1% TFA in methanol was applied as a gradient.

2-Amino-*N*-(2-(4-((((2S,3S,4R,5R)-5-(6-amino-9H-purin-9-yl)-3,4-dihydroxytetrahydrofuran-2-yl)methyl)thio)piperidin-1-yl)ethyl)-7,7-dimethyl-4-oxo-3,4,7,8-tetrahydropteridine-6-carboxamide (1): Synthesis of **1** was as described previously (11).

2-Amino-*N*-(2-((2-((((2S,3S,4R,5R)-5-(6-amino-9H-purin-9-yl)-3,4-dihydroxytetrahydrofuran-2-yl)methyl)sulfonyl)ethyl)amino)-2-oxoethyl)-7,7-dimethyl-4-oxo-3,4,7,8-tetrahydropteridine-6-carboxamide (2): Synthesis of **2** was as described previously (12).

2-Amino-*N*-(4-(2-((((2S,3S,4R,5R)-5-(6-amino-9H-purin-9-yl)-3,4-dihydroxytetrahydrofuran-2-yl)methyl)thio)ethyl)piperazin-1-yl)-7,7-dimethyl-4-oxo-3,4,7,8-tetrahydropteridine-6-carboxamide (3): To a solution of *t*-butyl (4-(2-hydroxyethyl)piperazin-1-yl)carbamate (0.1 mmol) in 20 mL CH_2Cl_2 was added triphenylphosphine (PPh_3) (0.11 mmol) and tetrabromomethane (CBr_4) (0.11 mmol). After stirring at 0 °C for 10 min, the reaction mixture was concentrated by rotary evaporation. The reaction mixture contained the *t*-butyl (4-(2-bromoethyl)piperazin-1-yl)carbamate and the compound was pure enough to proceed to the next step. 2',3'-*O*-isopropylideneadenosine-5'-thioacetate and *t*-butyl (4-(2-bromoethyl)piperazin-1-yl)carbamate were reacted according to General procedure A to result in *t*-butyl (4-(2-((((3aS,4S,6R,6aR)-6-(6-amino-9H-purin-9-yl)-2,2-dimethyltetrahydrofuro[3,4-d][1,3]dioxol-4-yl)methyl)thio)ethyl)piperazin-1-yl)carbamate. NMR′H δ (ppm) (700 MHz; CD_3OD), 1.47 (9 H, m), 1.58 (6 H, s), 2.88 (6H, m) 3.01 (6 H, m), 3.52 (2 H, t), 4.43 (1 H, m), 5.06 (1 H, m), 5.48 (1 H, m), 6.09 (1 H, m), 8.23 (1 H, s), 8.47(1 H, s). NMR′13C δ (ppm) (176 MHz; CD_3OD), 161.82 (1C), 157.60 (1C), 150.03 (1C), 147.97 (1C), 144.11 (1C), 121.17 (1C), 116.29 (1C), 92.09 (1C), 88.38 (1C), 85.75 (1C), 75.38 (1C), 57.08 (1C), 53.24 (1C), 52.93 (1C), 52.32 (1C), 52.13 (1C), 35.32 (1C), 28.89 (3C), 27.99 (1C), 27.68 (1C), 26.92 (1C), 25.72 (1C). MS (ESI-MS) calculated for $C_{24}H_{38}N_8O_5S$ (MH^+): 551.27; found: 551.30. Trifluoroacetic acid (TFA) (1 mL) was added dropwise at −20 °C to a solution of *t*-butyl (4-(2-((((3aS,4S,6R,6aR)-6-(6-amino-9H-purin-9-yl)-2,2-dimethyltetrahydrofuro[3,4-d][1,3]dioxol-4-yl)methyl)thio)ethyl)piperazin-1-yl)carbamate in CH_2Cl_2 (5 mL). Then, the mixture was stirred at room temperature overnight. After the reaction was finished, the solvent was removed under vacuum. The residue was purified by silica gel chromatography with CH_2Cl_2-methanol (0-20%), to afford (2R,3R,4S,5S)-2-(6-amino-9H-purin-9-yl)-5-(((2-(4-aminopiperazin-1-yl)ethyl)thio)methyl)tetrahydrofuran-3,4-diol. The compound was pure enough to proceed to the next step. It was reacted with 6-carboxy-7,7-dimethyl-7,8-dihydropterin according to General procedure B to provide the final product 2-amino-*N*-(4-(2-((((2S,3S,4R,5R)-5-(6-amino-9H-purin-9-yl)-3,4-dihydroxytetrahydrofuran-2-yl)methyl)thio)ethyl)piperazin-1-yl)-7,7-dimethyl-4-oxo-3,4,7,8-tetrahydropteridine-6-carboxamide (**3**). (22% yield, 95% purity) NMR′H δ (ppm) (700 MHz; CD_3OD), 1.61 (6 H, s), 2.68 (1 H, s), 2.72 (2 H, s), 2.88 (6H, m) 3.01 (6 H, m), 4.26 (1 H, m), 4.37 (1 H, m), 4.75 (1 H, m), 6.10 (1 H, d), 8.00 (2 H, s), 8.43 (1 H, s), 8.52 (1 H, s). NMR′13C δ (ppm) (176 MHz; CD3OD), 165.15 (1C), 164.07 (1C), 161.84 (1C), 157.16 (1C),

156.73 (1C), 153.18 (1C), 150.38 (1C), 147.21 (1C), 144.70 (1C),144.06 (1C), 121.00 (1C), 101.84 (1C), 91.00 (1C), 86.29 (1C), 75.35 (1C), 74.44 (1C), 57.21 (1C), 56.20 (1C), 53.11 (1C), 52.87 (1C), 37.25 (1C), 35.64 (1C), 35.48 (1C), 31.95 (1C), 29.50 (2C);MS (ESI-MS) calculated for $C_{25}H_{35}N_{13}O_5S$ (MH^+): 630.26; found: 630.30.

2-Amino-*N*-(2-(4-((((2S,3S,4R,5R)-5-(6-amino-9H-purin-9-yl)-3,4-dihydroxytetrahydrofuran-2-yl)methyl)thio)piperidin-1-yl)ethyl)-4-oxo-3,4-dihydropteridine-6-carboxamide (4): (2R,3R,4S,5S)-2-(6-amino-9H-purin-9-yl)-5-(((1-(2-aminoethyl)piperidin-4-yl)thio)methyl)tetrahydrofuran-3,4-diol was synthesized as described previously (11). It was reacted with 6-pteridinecarboxylic acid according to General procedure B to provide 2-amino-*N*-(2-(4-((((2S,3S,4R,5R)-5-(6-amino-9H-purin-9-yl)-3,4-dihydroxytetrahydrofuran-2-yl)methyl)thio)piperidin-1-yl)ethyl)-4-oxo-3,4-dihydropteridine-6-carboxamide (**4**). (20% yield, 95% purity) MS (ESI-MS) calculated for $C_{24}H_{30}N_{12}O_5S$ (MH^+): 599.22; found: 599.30.

2-Amino-*N*-(1-(2-((((2S,3S,4R,5R)-5-(6-amino-9H-purin-9-yl)-3,4-dihydroxytetrahydrofuran-2-yl)methyl)sulfonyl)ethyl)piperidin-4-yl)-7,7-dimethyl-4-oxo-3,4,7,8-tetrahydropteridine-6-carboxamide (5): *S*-(2-(4-((*t*-butoxycarbonyl)amino)piperidin-1-yl)ethyl) ethanethioate was reacted with 2',3'-O-isopropylidene-5'-*O*-tosyladenosine (0.1 mmol) according to General procedure A to result in *t*-butyl-(1-(2-((((3aS,4S,6R,6aR)-6-(6-amino-9H-purin-9-yl)-2,2-dimethyltetrahydrofuro[3,4-d][1,3]dioxol-4-yl)methyl)thio)ethyl)piperidin-4-yl)carbamate. This compound was oxidized with oxone (0.3 mmol) in MeOH and the BOC group was removed by TFA/CH_2Cl_2 (1 mL/5 mL) to yield (2R,3R,4S,5S)-2-(6-amino-9H-purin-9-yl)-5-(((2-(4-aminopiperidin-1-yl)ethyl)sulfonyl)methyl)tetrahydrofuran-3,4-diol. It was reacted with 6-carboxy-7,7-dimethyl-7,8-dihydropterin according to General procedure A to provide 2-amino-*N*-(1-(2-((((2S,3S,4R,5R)-5-(6-amino-9H-purin-9-yl)-3,4-dihydroxytetrahydrofuran-2-yl)methyl)sulfonyl)ethyl)piperidin-4-yl)-7,7-dimethyl-4-oxo-3,4,7,8-tetrahydropteridine-6-carboxamide (**5**). (18% yield, 95% purity) **(**MS (ESI-MS) calculated for $C_{26}H_{36}N_{12}O_7S$ (MH^+): 661.26; found: 661.30. NMR′H (400 MHz; CD_3OD), 1.56 (6H, s), 1.80 (4H, m), 2.05 (4H, m), 3.09 (2H, m), 3.63-3.45 (3H, m), 3.85-3.98 (3H, m), 4.45 (1H, m), 4.52 (1H, m), 4.75 (1H, m), 6.10 (1H, d), 6.79 (1H, s) 6.92 (1H, s), 7.97 (1H, s), 8.41 (1H, s), 8.45 (1H, s). NMR′13C δ (100 MHz; CD_3OD), 165.67 (1C), 165.18 (1C), 163.11 (1C), 161.85 (1C), 158.49 (1C), 157.11 (1C), 156.76 (1C), 150.35 (1C), 143.92 (1C), 121.38 (1C), 101.77 (1C), 91.93 (1C), 80.60 (1C), 74.87 (1C), 74.51 (1C), 58.13 (1C), 55.25 (1C), 40.73 (3C), 35.74 (2C), 37.26 (1C), 30.71 (1C), 29.62 (2C).

2,2'-(((2-hydroxybutane-1,4-diyl)Bis(oxy))bis(3-bromo-4,1-phenylene))bis(1H-benzo[d]imidazole-6-carboxylic acid) (6): Synthesis of **6** was as previously described (3).

2,2'-(((1,2-phenylenebis(methylene))Bis(oxy))bis(4,1-phenylene))bis(1H-benzo[d]imidazole-5-carboxylic acid) (7): Synthesis of **7** was as previously described (3).

References

1. Shaw GX, Li Y, Shi G, Wu Y, Cherry S, Needle D, et al. Structural enzymology and inhibition of the bi-functional folate pathway enzyme HPPK-DHPS from the biowarfare agent Francisella tularensis. FEBS J. 2014;281(18):4123-37.
2. Blakley RL. Crystalline Dihydropteroylglutamic Acid. Nature. 1960;188(4746):231-2.
3. Toulouse JL, Yachnin BJ, Ruediger EH, Deon D, Gagnon M, Saint-Jacques K, et al. Structure-Based Design of Dimeric Bisbenzimidazole Inhibitors to an Emergent Trimethoprim-Resistant Type II Dihydrofolate Reductase Guides the Design of Monomeric Analogues. ACS Omega. 2019;4(6):10056-69.
4. Toulouse JL, Edens TJ, Alejaldre L, Manges AR, Pelletier JN. Integron-associated DfrB4, a previously uncharacterized member of the trimethoprim-resistant dihydrofolate reductase B family, is a clinically identified emergent source of antibiotic resistance. Antimicrob Agents Chemother. 2017;61:1-5.
5. Schmitzer AR, Lépine F, Pelletier JN. Combinatorial exploration of the catalytic site of a drug-resistant dihydrofolate reductase: Creating alternative functional configurations. Protein Eng Des Sel. 2004;17:809-19.
6. Studier FW. Protein production by auto-induction in high density shaking cultures. Protein Expression and Purification. 2005;41(1):207-34.
7. Toulouse JL, Abraham SMJ, Kadnikova N, Bastien D, Gauchot V, Schmitzer AR, et al. Investigation of classical organic and ionic liquid cosolvents for early-stage screening in fragment-based inhibitor design with unrelated bacterial and human dihydrofolate reductases. Assay Drug Dev Technol. 2017;15:141-53.
8. Cheng Y, Prusoff WH. Relationship between the inhibition constant and the concentration of inhbitor which causes 50 percent inhibition of an enzymatic reaction. Biochemical Pharmacology. 1973;22:3099-108.
9. Bastien D, Ebert MC, Forge D, Toulouse J, Kadnikova N, Perron F, et al. Fragment-based design of symmetrical bis-benzimidazoles as selective inhibitors of the trimethoprim-resistant, type II R67 dihydrofolate reductase. J Med Chem. 2012;55(7):3182-92.
10. Labute P. LowModeMD--implicit low-mode velocity filtering applied to conformational search of macrocycles and protein loops. J Chem Inf Model. 2010;50(5):792-800.
11. Shi G, Shaw G, Liang YH, Subburaman P, Li Y, Wu Y, et al. Bisubstrate analogue inhibitors of 6-hydroxymethyl-7,8-dihydropterin pyrophosphokinase: New design with improved properties. Bioorganic and Medicinal Chemistry. 2012;20:47-57.
12. Shi G, Shaw G, Li Y, Wu Y, Yan H, Ji X. Bisubstrate analog inhibitors of 6-hydroxymethyl-7,8-dihydropterin pyrophosphokinase: New lead exhibits a distinct binding mode. Bioorganic and Medicinal Chemistry. 2012;20:4303-9.